Solution Structure of the Cytoplasmic Domain of the Human CD4 Glycoprotein by CD and ^{1}H NMR Spectroscopy: Implications for Biological Functions

Victor Wray,*[,‡] Dirk Mertins,[‡,§] Michael Kiess,[‡] Peter Henklein,[||] Wolfram Trowitzsch-Kienast,[§] and Ulrich Schubert[⊥,#]

Department of Molecular Structure Research, Gesellschaft für Biotechnologische Forschung, 38124 Braunschweig, Germany, Department of Chemistry, Technische Fachhochschule, 13353 Berlin, Germany, Institute of Pharmacology and Toxicology, Faculty of Medicine, Humboldt University, 10117 Berlin, Germany, Laboratory of Molecular Microbiology, National Institute of Allergy and Infectious Diseases, National Institutes of Health, 4/312, Bethesda, Maryland 20892-0440, and Heinrich-Pette-Institute of Experimental Virology, University of Hamburg, 20251 Hamburg, Germany

Received September 16, 1997; Revised Manuscript Received April 10, 1998

ABSTRACT: The human T cell receptor CD4 is a type I integral membrane glycoprotein that is involved in T cell activation and also acts as the primary coreceptor for human immunodeficiency viruses (HIV). Here the structure of a synthetic 38 amino acid peptide corresponding to the complete cytoplasmic domain of CD4 ($CD4_{CYTO}$) has been investigated under a variety of solution conditions using a combination of circular dichroism and homonuclear two-dimensional ^{1}H nuclear magnetic resonance spectroscopy. In the presence of the membrane mimetic 2,2,2-trifluoroethanol (TFE), a conformational change of $CD4_{CYTO}$ from a random coil to an α-helical structure was observed. In keeping with this, $CD4_{CYTO}$ has the potential to associate with membranes as demonstrated by binding studies of in vitro phosphorylated $CD4_{CYTO}$ with microsomal membranes. Both chemical shift and nuclear Overhauser enhancement data in 50% 2,2,2-trifluoroethanol solution provide direct experimental evidence for the predominance of a short amphiphatic α-helix that is approximately 4 turns in length and extends from positions Arg-402 to Lys-417. The present data provide, for the first time, compelling experimental evidence that only a fraction of $CD4_{CYTO}$ has a propensity for adopting secondary structure under conditions that are assumed to exist at or near to the membrane surface and that this α-helical structure is located in the membrane-proximal region of $CD4_{CYTO}$. The N-terminal residues, that link the α-helix to the transmembrane anchor of CD4, and a substantial C-terminal portion (14−18 residues) of $CD4_{CYTO}$ are unstructured under the solution conditions investigated. Correlation of our structural data with recent studies on the biological activity of $CD4_{CYTO}$ indicates that the α-helix is of crucial importance for the interaction of CD4 with Nef and Vpu in the process of HIV-mediated CD4 down-regulation.

The cell surface receptor CD4 is a 55 kDa type I integral membrane glycoprotein which is expressed on the surface of a subset of T lymphocytes that recognize MHC[1] class II presented antigens (Ag) (*1*). Beside its pivotal function in the development and maintenance of the immune system, CD4 is also an essential coreceptor for HIV-1 entry and plays a central role in the pathogenesis of AIDS (*1*, *2*). The human CD4 molecule is comprised of a 370 amino acid extracellular ($CD4_{ECTO}$) domain, a single 25 amino acid transmembrane ($CD4_{TM}$) anchor, and a cytoplasmic ($CD4_{CYTO}$) tail of 38 amino acids. Structural analysis of CD4 by X-ray crystallography has been focused on the soluble $CD4_{ECTO}$ domain because of the technical difficulties associated with crystallizing complete transmembrane glycoproteins. On the other hand, studies on the full-length CD4 molecule in a membrane system by solid-state NMR techniques are currently impractical because of the size of the proteins involved.

Apart from secondary structure predictions (*3*−*5*), little structural analysis has been addressed to the $CD4_{CYTO}$ tail, even though this membrane-proximal region has important biological functions. First, following interaction of the $CD4_{ECTO}$ domain with the MHC class II Ag−TCR complex, the activation cascade of T cell response is transmitted to the cytoplasm via noncovalent binding of the $CD4_{CYTO}$ tail with the tyrosine kinase $p56^{lck}$, a member of the *src* family of cytosolic tyrosine kinases (*1*, *6*). This interaction, which is mediated through a di-cysteine motif, residues 419-CQC-

* Correspondence should be addressed to this author at Abteilung für Strukturforschung, GBF−Gesellschaft für Biotechnologische Forschung mbH, Mascheroder Weg 1, D-38124 Braunschweig, Germany. Fax: +531 6181 355. E-mail: vwr@gbf-braunschweig.de.

‡ Gesellschaft für Biotechnologische Forschung.

§ Technische Fachhochschule.

|| Humboldt University.

⊥ National Institute of Allergy and Infectious Diseases.

University of Hamburg.

[1] Abbreviations: Ag, antigen; AIDS, acquired immunodeficiency syndrome; CD, circular dichroism; $CD4_{ECTO}$, extracellular domain of CD4; $CD4_{CYTO}$, cytoplasmic domain of CD4; $CD4_{TM}$, transmembrane domain of CD4; COSY, correlation spectroscopy; DTT, dithiothreitol; ER, endoplasmic reticulum; HIV, human immunodeficiency virus; MEM, membrane; MHC, major histocompatibility complex; NMR, nuclear magnetic resonance; NOE, nuclear Overhauser enhancement; NOESY, nuclear Overhauser and exchange spectroscopy; PBS, phosphate-buffered saline; PKC, protein kinase C; RMS, root-mean-square; SDS−PAGE, sodium dodecyl sulfate−polyacrylamide gel electrophoresis; SUP, supernatant; TFE, 2,2,2-trifluoroethanol; TOCSY, total correlation spectroscopy; Ub, ubiquitin; Vpu_{CYTO}, cytoplasmic domain of Vpu.

S0006-2960(97)02311-8 CCC: $15.00
Published on Web 05/22/1998

423 (*7*), and a predicted α-helical structure (*4*) within $CD4_{CYTO}$, is required for T cell activation upon Ag recognition (*8*). Both stimulation by Ag exposure and treatment with phorbol ester induce protein kinase-dependent phosphorylation of three serine residues in the $CD4_{CYTO}$ tail (*9*) which triggers dissociation of $p56^{lck}$ from CD4 followed by internalization and lysosomal degradation of CD4 (*10*). Second, another important function of the $CD4_{CYTO}$ tail is the interaction with the HIV accessory proteins Nef and Vpu occurring in the complex process of HIV receptor interference (*1*, *6*, *11*). Down-regulation of the primary virus receptor CD4 in HIV-infected cells, a hallmark occurring in many retrovirus systems, is mediated through at least three independent mechanisms: (i) The virus envelope precursor protein gp160 allows the formation of stable complexes with newly synthesized CD4, resulting in the entrapment of both CD4 and Env in the endoplasmic reticulum (ER) (*12*, *13*); (ii) the HIV-1-specific accessory protein Vpu induces a selective and rapid destruction of CD4 trapped in the ER and, therefore, enhances at the same time transport and processing of Env glycoproteins (*14*, *15*); and (iii) the HIV accessory protein Nef expressed prior to the 'late' viral products Env and Vpu in the viral replication cycle induces down-regulation of CD4 from the cell surface by increased endocytosis via clathrin-coated pits followed by lysosomal degradation (*11*, *16*−*19*). While the first mechanism requires binding between the extracellular domains of CD4 and gp60, Nef and Vpu specifically target the $CD4_{CYTO}$ tail. The minimal Vpu responsive element in the $CD4_{CYTO}$ tail was defined as a region comprising residues 414-LSEKKT-419 (*20*−*23*), while for Nef-mediated CD4 down-regulation a di-leucine motif in position 412-LL-415 is important (*16*). In addition, several reports indicate the requirement of a putative α-helical conformation in the proximal part of $CD4_{CYTO}$ for interaction with Vpu (*5*, *24*), Nef (*4*), and also $p56^{lck}$ (*4*). Previous studies have shown that a region of $CD4_{CYTO}$ encompassing Lys^{418} to Ile^{433} is involved in the binding to $p56^{lck}$ (*25*). Subsequent studies have suggested that this membrane-proximal region of $CD4_{CYTO}$ should have a putative α-helical structure and is, furthermore, necessary for internalization and lysosomal targeting of CD4 (*3*, *9*). Secondary structure prediction revealed one extended α-helical conformation within the $CD4_{CYTO}$ domain extending from Arg^{402} to Thr^{419} (*3*, *5*, *9*, *24*). Mutations introduced to disrupt this hypothetical α-helical structure resulted in the loss of susceptibility of the CD4 molecule to down-regulation by Nef (*4*) and Vpu (*5*, *24*), or its association with $p56^{lck}$ (*4*). Taken together, these studies suggest that, in addition to specific amino acid sequence motifs, a structural element in the $CD4_{CYTO}$ domain is important for the biological function of CD4, i.e., T cell activation and HIV-mediated receptor interference. To date, however, no experimental structural analysis at the atomic level has been undertaken of the complete $CD4_{CYTO}$ domain.

In the present study, we analyzed the solution structure of a synthetic 38 amino acid peptide comprising the entire $CD4_{CYTO}$ domain (R^{396} to I^{433}) by multidimensional ^1H NMR and circular dichroism spectroscopy. We found that upon addition of trifluoroethanol the molecule assumes an amphipathic α-helix that is centered between Gln-403 and Ser-415. This is followed by a C-terminal region of approximately equal length that shows no tendency to adopt a defined structure under the solution conditions investigated. The transition of structured to nonstructured region occurs prior to the di-cysteine motif 419-CQC-423 which is important for interaction with $p56^{lck}$ during T cell activation (*7*). Therefore, while the α-helical region in $CD4_{CYTO}$ covers the target sites for the HIV factors Nef and Vpu, the binding site for $p56^{lck}$ resides in the nonstructured C-terminal end.

MATERIALS AND METHODS

Peptide Synthesis, Purification, Sequencing, and Mass Spectrometry. The peptide $CD4_{CYTO}$ comprising the entire cytoplasmic tail of human CD4, residues R^{396} to I^{433} (*26*), was synthesized as the C-terminal amide on an ABI 433A Peptide Synthesizer (Applied Biosystems, Weiterstadt, Germany) with conductivity feedback montoring using Fmoc strategy with minor changes to the standard protocol and TentaGel R-RAM resin (Rapp Polymere, Tübingen, Germany). The Fmoc amino acids had the following side chain protecting groups: Arg (Pmc), Asp (OtBu), Glu (OtBu), Lys (Boc), Ser (tBu), Asn (Trt), Gln (Trt), Cys (Trt). The peptide was cleaved from the resin with TFA/EDT/water/triisopropylsilane (85:7:5:3) for 4 h and was purified by reverse-phase HPLC (LC8, Shimadzu, Kyoto, Japan) with a 300 × 40 mm VYDAC TPB 1520 300 Å C18 reverse phase column at a flow rate of 1.00 mL/min. The purity of the peptide was checked by sequencing, and the molecular weight was established by negative-ion electrospray ionization mass spectrometry.

In Vitro Phosphorylation of $CD4_{CYTO}$. A 12.5 μg aliquot of $CD4_{CYTO}$ was incubated in 40 μL of phosphorylation buffer (20 mM Tris/HCl, pH 7.5, 10 mM $MgCl_2$, 1 mM $CaCl_2$, 1 mM DTT) containing 10 μCi of [γ-^{32}P]ATP and 0.16 milliunit of protein kinase C (PKC, Ca^{2+}-activated, EC 2.7.1.37; Boehringer Mannheim, Indianapolis, IN) for 30 min at 30 °C. The reaction was terminated by the addition of 200 ng of the PKC inhibitor bis(indolylmaleimide) (Boehringer Mannheim). The reaction mixture was aliquoted and frozen at −80 °C.

Quantitation of Membrane Association of $CD4_{CYTO}$. A 1.5 μg sample of in vitro phosphorylated $CD4_{CYTO}$ was incubated with 5 μL of microsomal membranes (Promega, Madison, WI) in 100 μL of PBS (150 mM NaCl, 10 mM KP_i, pH 7.4) for 30 min at 25 °C with gentle shaking. The membrane fraction was isolated by centrifugation (30 min, 100000*g*, 4 °C) onto a sucrose cushion; 95 μL of the supernatant was added to 305 μL of Triton wash buffer (0.5% Triton X-100, 10 mM Tris/HCl, pH 7.4, 300 mM NaCl) to give the supernatant (SUP) fraction. The sucrose cushion was dissolved in 350 μL of PBS, and the membranes were finally isolated by centrifugation (60 min, 100000*g*, 4 °C). The supernatant from the second centrifugation step was decanted to give the wash (WASH) fraction. The membrane pellet was dissolved in 400 μL of Triton wash buffer to give the membrane (MEM) fraction. The amount of membrane-associated, phosphorylated $CD4_{CYTO}$ was evaluated by three different methods: (i) aliquots of the SUP, WASH, and MEM fractions were spotted onto DEAE-cellulose (Wallace, Turku, Finland), dried for 30 min at 80 °C, washed twice with 10% trichloroacetate (TCA) and once with 70% ethanol, and finally air-dried. The radioactivity was estimated using a 1450 Microbeta Scintillation Counter (Wallace). To

quantitate the radioactivity of the isolated $CD4_{CYTO}$, (ii) either the peptide was immunoprecipitated with polyclonal (rabbit) antibodies directed against $CD4_{CYTO}$, or (iii) aliquots of the SUP, WASH, and MEM fractions were loaded directly onto a 16% SDS−acrylamide gel. Gels were fixed for 30 min by incubation in 40% methanol and 10% acetic acid, rinsed with water, soaked in 1 M sodium salicylic acid for 30 min, and dried. Radioactive bands were visualized by fluorography. Estimation of fluorograms was performed using the phosphor-image-analyzer STORM 860 and the ImageQuant Software (Molecular Dynamics Inc., Sunnyvale, CA).

Antibodies and Immunoprecipitation. A rabbit polyclonal antiserum directed against $CD4_{CYTO}$ tail was raised to keyhole limpet hemocytanin coupled to the peptide $CD4_{CYTO}$. Immunoprecipitation of $CD4_{CYTO}$ was performed according to a procedure described previously (*27*). Briefly, aliquots of the SUP, WASH, and MEM fractions were diluted 1:3 in Triton wash buffer and precleared with preimmune serum (rabbit) bound to GammaBind-Plus-Sepharose beads (Pharmacia LKB, Pitscataway, NJ) followed by immunoprecipitation with anti-$CD4_{CYTO}$ antibodies preloaded onto GammaBind-Plus-Sepharose beads. The immunoprecipitates were washed twice with Triton wash buffer and once with SDS−DOC buffer (50 mM Tris/HCl, pH 7.4, 300 mM NaCl, 0.1% SDS, 0.1% deoxycholate), boiled for 10 min at 95 °C in sample buffer (2% SDS, 1% mercaptoethanol, 1% glycerol, 65 mM Tris/HCl, pH 6.8), and separated in 16% SDS−acrylamide gels (FMC Corporation Bio Products, Philadelphia, PA).

CD and NMR Spectroscopy. CD spectra were recorded at ambient temperature on a Jasco J-600 spectropolarimeter (Jasco, Tokyo, Japan). Samples of the peptide (9 mg) for NMR measurements were dissolved in 50% TFE-d_2 by volume to give a final volume of 600 μL at pH 1.9 [TFE-d_2 was produced by fractional distillation of a 1:1 mixture of deionized H_2O and TFE-d_3 (Merck, Darmstadt, Germany)]. A small amount (0.3 mg) of 1,4-dithiothreitol (Sigma, Deisenhofen, Germany) was added to prevent oxidation of the four cysteine residues, and nitrogen was bubbled through the peptide solution to remove oxygen. Spectra were recorded at 300 K on a Bruker DMX 600 without spinning using a dedicated 5 mm proton probehead and temperature unit (Haake, Karlsruhe, Germany). The ^{1}H spectra were referenced to sodium 4,4-dimethyl-4-silapentane-1-sulfonate and indirectly to the residual signal of TFE at 3.95 ppm. 2D phase-sensitive ^{1}H COSY, TOCSY (mixing times 110 ms), and NOESY (mixing times 250 ms) spectra were recorded and processed as described previously (*28*).

Structure Calculations. The volumes of the integrated cross-peaks from the NOESY spectra were determined using the AURELIA program (*29*) operating under UNIX on an INDIGO workstation (Silicon Graphics, CA). The side-chain amide protons of the Gln residues were not sufficiently well resolved to allow suitable calibration of the NOE data. However, as the pattern of (i, i+3) and (i, i+4) NOEs and chemical shift data (Figure 4) are strong evidence for the presence of an α-helical structure in at least the region around residues 16−20, we have calibrated the NOE data against those of the averaged NH−NH NOEs for these residues which were taken as 0.33 nm (the value pertaining in an α-helix). The consequences of doing this are discussed below.

After correction for pseudoatoms, where appropriate, these values were used directly as distance restraints in molecular dynamics calculations using the program X-PLOR version 3.1 (*30*) on a DEC VAX 3000 Alpha workstation (Digital Equipment Corp., Maynard, MA). An initial structure was calculated using randomized backbone dihedral angles and a short MD calculation at 300 K. The following simulated annealing calculation (*31*), using floating stereospecific assignment (*32*), incorporated the following stages. After a short energy minimization, the first stage started with scaling of the weights of the NOE, constrained improper dihedrals, and nonbonded terms from initially small values to more realistic ones using in total 15 000 time steps each of 0.005 ps at 2000 K. The second stage performed a slow cooling of the system to 100 K in 38 stages each with ca. 150 time steps of 0.005 ps. The final stage consisted of 800 cycles of energy minimization. Floating stereospecific assignment was used because of the difficulties in achieving a priori stereospecific assignments. The resulting structures were displayed on a Hewlett-Packard Apollo graphic workstation (Hewlett-Packard Co., Palo Alto, CA) using the program BRAGI (Version 5.0) (*33*). Structure fitting criteria were objectively derived using a consecutive segment method described by us previously (*34*) that employs modified programs from X-PLOR.

RESULTS

Synthesis, Purification, and Characterization of $CD4_{CYTO}$. To investigate the solution structure of human $CD4_{CYTO}$, a 38 amino acid peptide comprising the entire CD4 cytoplasmic domain of human CD4 (*26*) from residue R^{397} to residue I^{433} (for sequence, see Figure 7) has been synthesized using Fmoc chemistry. The crude peptide was purified by reverse-phase HPLC, and the identity of the peptide $CD4_{CYTO}$ was established by amino acid analysis, partial N-terminal sequence analysis, and negative-ion electrospray ionization mass spectrometry. The mass of the deconvoluted molecular ion of 4696 Da agreed well with the precise molecular mass of 4697.6 Da calculated for the peptide. The homogeneity of the product was established by HPLC and confirmed by 1D ^{1}H NMR spectroscopy, where there was no evidence of any substantial amounts of contaminating byproducts.

CD Spectroscopy of $CD4_{CYTO}$. To define optimal solution conditions for subsequent NMR experiments and to obtain information about secondary structures adopted by $CD4_{CYTO}$ in solution, we analyzed the peptide by CD spectroscopy in aqueous solution containing increasing percentages of TFE. This organic solvent was chosen as it appears to invoke the same types of conformation change in structurally labile peptides that are afforded by lipid bilayers and micelles, the environments of which are assumed to pertain at or near the membrane surface and hence influence the structure of molecules bound to the membrane (*35*).

In the absence of TFE, the initial shallow negative CD curve with a minimum at ca. 200 nm and a very small negative ellipticity value at 220 nm was characteristic of a disordered peptide conformation with very little evidence of stable secondary structure (Figure 1). Addition of TFE caused a pronounced shift in the initial minimum to 206 nm, and simultaneously a second substantial negative ellipticity

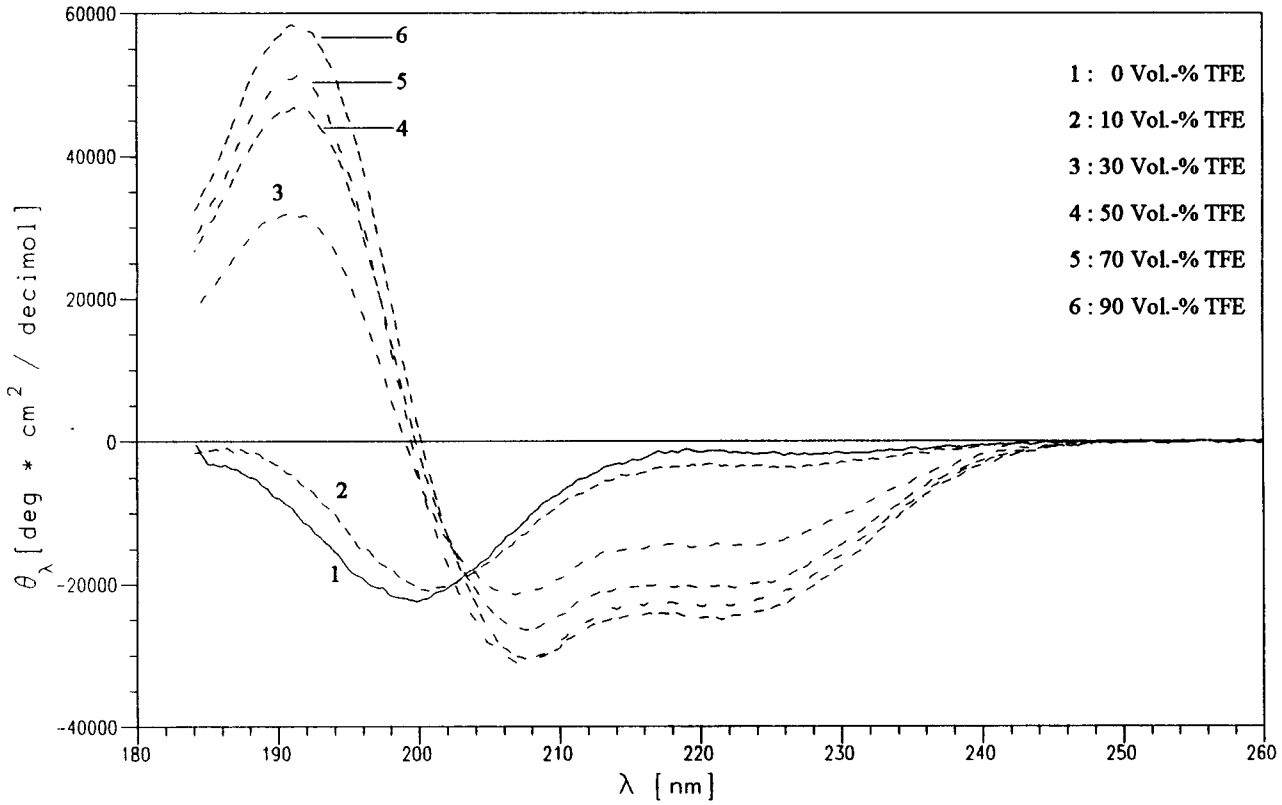

FIGURE 1: CD spectra of $CD4_{CYTO}$ in aqueous solution containing TFE.

developed at ca. 220 nm and a positive band at 190 nm, that were indicative of an increasing content of stable α-helical secondary structure. The most pronounced changes were observed on going from 0 to 30% TFE and were less pronounced thereafter, suggesting that the peptide adopts a limiting stable structure that is only little affected by further addition of organic solvent. As a result of the CD analyses, all subsequent NMR experiments were performed in 50% aqueous TFE.

$CD4_{CYTO}$ Association with Membranes. Our CD analysis indicates that $CD4_{CYTO}$ adopts a stable secondary structure only when a membrane-like environment was present. Hence, the relevance of this structure may be questioned as intuitively it is believed that the C-terminal domain of CD4 is oriented solely into the cytoplasmic space. To clarify whether the cytoplasmic tail, in addition to the transmembrane anchor, interacts with the membrane, we studied the potential of the peptide $CD4_{CYTO}$ to associate with microsomal membranes. Since CD4 is phosphorylated in vivo by protein kinase C (PKC) at seryl residues 408, 415, and 431 in the process of T cell activation following Ag recognition (*1*, *8*, *9*), we utilized this posttranslational modification to achieve the sensitivity necessary for detection of the peptide $CD4_{CYTO}$ in our assay. Following in vitro phosphorylation of $CD4_{CYTO}$ with PKC and [γ-^{32}P]ATP, the kinase activity was inactivated with the PKC inhibitor bis(indolylmaleimide) to prevent unspecific phosphorylation of proteins associated with the microsomal membranes. The phosphorylated peptide, designated $CD4_{CYTO}$*, was incubated with canine microsomal membranes in PBS, and the fraction of $CD4_{CYTO}$* that remains membrane-associated was estimated following a two-step centrifugation protocol outlined in Figure 2A. The relative amounts of $CD4_{CYTO}$* in the resulting supernatant (SUP), wash (WASH), and membrane pellet (MEM) fractions were estimated by counting the radioactivity of TCA-precipitated material (Figure 2C) or by separation of $CD4_{CYTO}$* in a denaturing SDS−PAGE (Figure 2B,C). In the first gel analysis, aliquots of the SUP, WASH, and MEM fractions were loaded directly onto the gel. Radioactive bands migrating at the expected molecular weight of the radiolabeled peptide $CD4_{CYTO}$* were detected by fluorography (Figure 2B, first panel). The quantitation of the radioactivity in each of the bands by phosphor image analysis revealed that 71% of $CD4_{CYTO}$* was membrane-associated, while 7% and 22% were detected in the WASH and SUP fractions, respectively (Figure 2C, first panel). This result was consistent with that of the TCA precipitation where the distribution of $CD4_{CYTO}$* was 68% in the MEM, 8% in the WASH, and 24% in the SUP fraction (Figure 2C, third panel). To evaluate the specificity of the detection of $CD4_{CYTO}$*, aliquots of each fraction were subjected to immunoprecipitation using anti-$CD4_{CYTO}$ antibodies followed by SDS−PAGE (Figure 2B, second panel). Similar to previous results, quantitation of $CD4_{CYTO}$* (Figure 2C, second panel) revealed 59% in the MEM, 12% in the SUP, and 29% in the WASH fractions.

The increase in the relative amount of membrane-associated $CD4_{CYTO}$* detected by direct loading onto SDS−PAGE compared to that isolated by immunoprecipitation prior to its separation by SDS−PAGE may reflect potential dephosphorylation of $CD4_{CYTO}$* that could occur during the precipitation procedure by the action of phosphatases associated with microsomal membranes. Furthermore, in our membrane binding studies, we could only evaluate the distribution of phosphorylated peptide but not that of the nonphosphorylated $CD4_{CYTO}$. Further analyses are necessary to determine the effect of phosphoseryl residues for membrane interaction of $CD4_{CYTO}$.

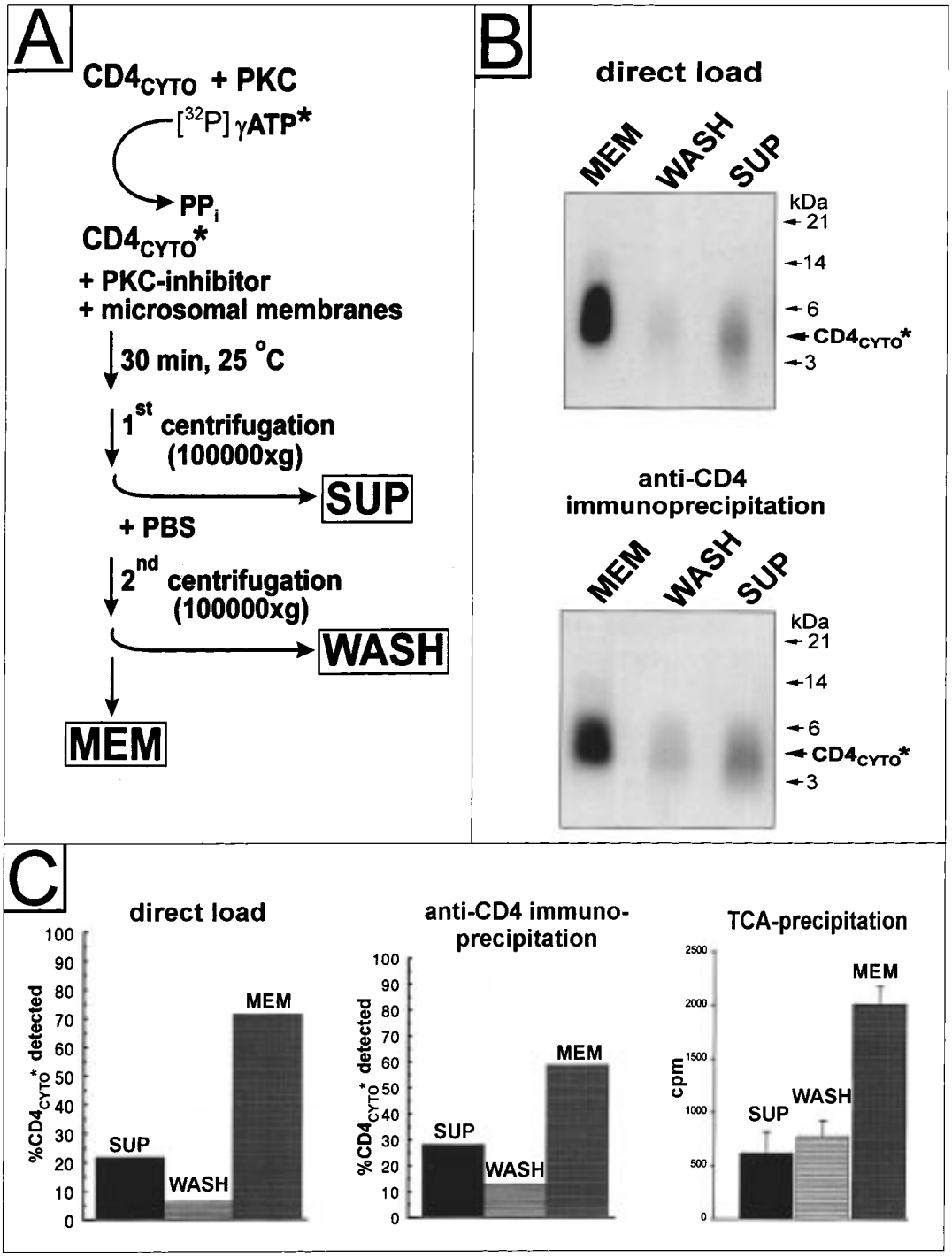

FIGURE 2: $CD4_{CYTO}$ has the potential to associate with membranes. The peptide $CD4_{CYTO}$ was in vitro phosphorylated with PKC and [γ-^{32}P]ATP, resulting in $CD4_{CYTO}$*. Incubation of $CD4_{CYTO}$* with microsomal membranes and separation into SUP, WASH, and MEM fractions are schematically outlined in (A) and described in detail in the text. Aliquots of each fraction were separated by SDS−PAGE (B), by either directly loading onto the gel or after immunoprecipitation with anti-$CD4_{CYTO}$ antibodies. Positions of molecular mass standards and $CD4_{CYTO}$* are indicated on the right. Only parts of the fluorograms in the range 2−46 kDa are shown. Relative amounts of membrane-associated $CD4_{CYTO}$* were estimated (C) by phosphor image analysis of fluorograms shown in (B) or by scintillation counting of TCA-precipitated peptide $CD4_{CYTO}$*. A representative result of repeated experiments is shown in (B) and (C). Quantitation of TCA-precipitated $CD4_{CYTO}$* was performed in parallel 6 times (C).

In summary, the combined results indicate that approximately 60−70% of $CD4_{CYTO}$* remains associated with microsomal membranes, suggesting that the phosphorylated cytoplasmic tail of CD4 has the potential of associating with membranes.

^{1}H NMR Spectroscopy of $CD4_{CYTO}$. Although disulfide bond formation in the CD4 molecule has been described for $CD4_{ECTO}$, it has not been found in the $CD4_{CYTO}$ domain which contains four cysteine residues in positions 397, 420, 422, and 430. Precautions were necessary to avoid autoxidation of the cysteines as we observed problems with the solubility of the peptide under nonreducing conditions, especially after a number of freeze-dry cycles. The autoxidation problem of $CD4_{CYTO}$ became particularly apparent

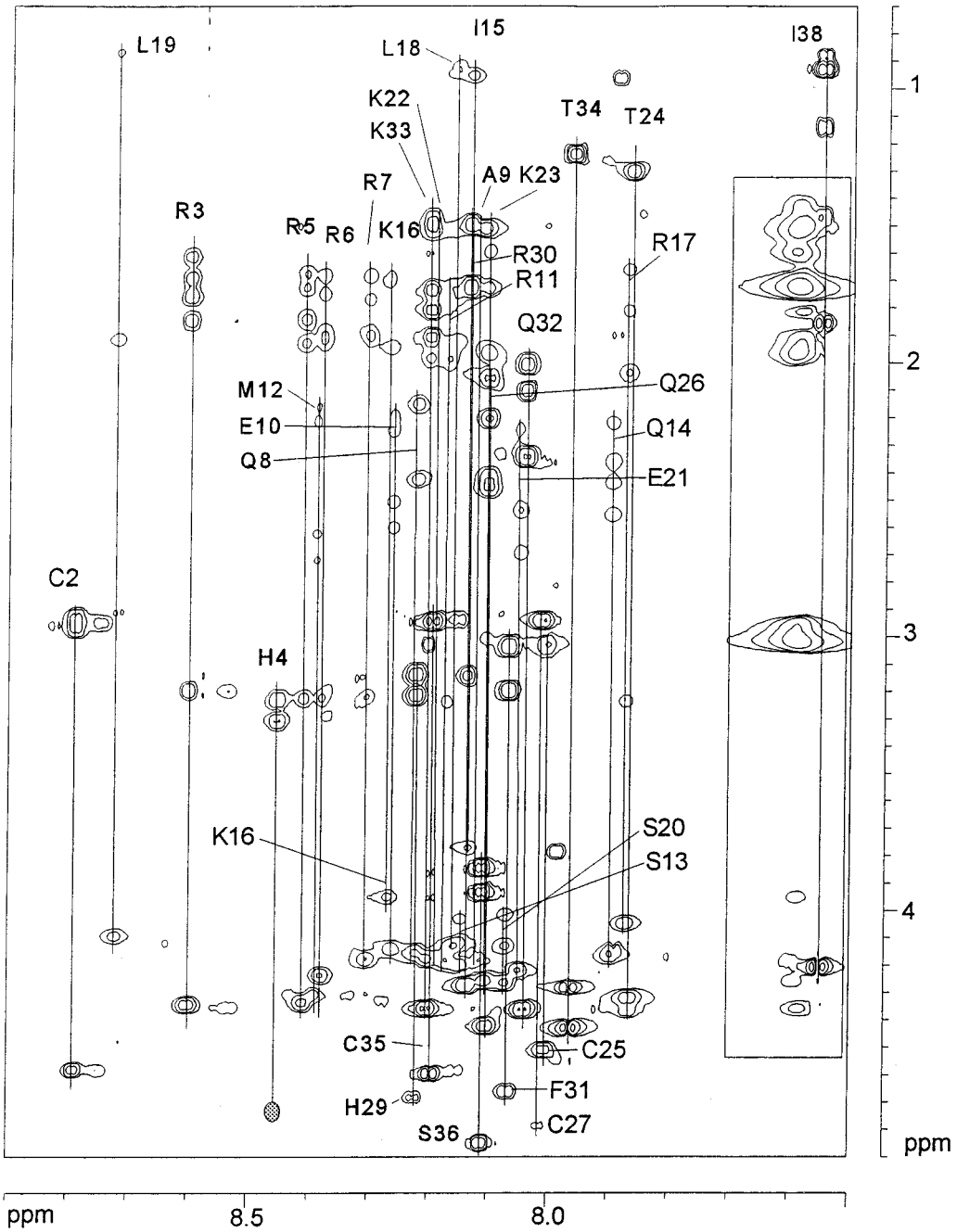

FIGURE 3: Amino acid spin systems of the NH region of the 2D TOCSY spectrum (mixing time, 110 ms) of a 3 mM solution of $CD4_{CYTO}$ in 1:1 (v/v) TFE-d_2/H_2O at 300 K and pH 1.9, containing a small amount of 1,4-dithiothreitol (0.3 mg/600 μL). Arg-1, Pro-28, and Pro-37 show no signals in this region, and the signal of His-4 shown as an oval is not visible as it lies under the irradiated residual water signal.

from the occurrence of multiple signals in the ^{1}H NMR spectra especially in the vicinity of the cysteine residues. Addition of an equimolar concentration of DTT and removal of oxygen by a stream of nitrogen afforded a stable peptide solution that provided readily interpretable ^{1}H NMR spectra.

The through-bond connectivities of the various amino acid spin systems were identified from 2D ^{1}H phase-sensitive COSY and TOCSY spectra starting from the amide protons in the region 8.9−7.5 ppm, and were confirmed by inspection of cross-peaks in the high-field region corresponding to side-chain connectivities. Sequence-specific assignments then followed from sequential NOE signals in the NOESY spectra that reflect the short through-space distances between HN, Hα, and Hβ of amino acid i and HN of amino acid i+1. An almost complete sequence was determined from the "fingerprint" region of the NOESY spectrum involving HN and Hα that was confirmed from other spectral regions involving interactions between neighboring NHs and from these with Hβ. The full sequential assignments are shown on the TOCSY spectrum (Figure 3). Subsequently, additional confirmation of the sequence assignments was provided by medium-range NOE's in the regions of secondary structure where Hα−Hβ(i,i+3) and Hα−HN(i,i+3) NOE's were observed. The complete signal assignments and shifts are available.

Secondary Structure from Hα Chemical Shifts and Qualitative NOEs. The Hα chemical shifts are strongly dependent on the nature of protein secondary structure in both proteins and peptides with an upfield shift relative to the random coil value being indicative of helices and a downfield shift of

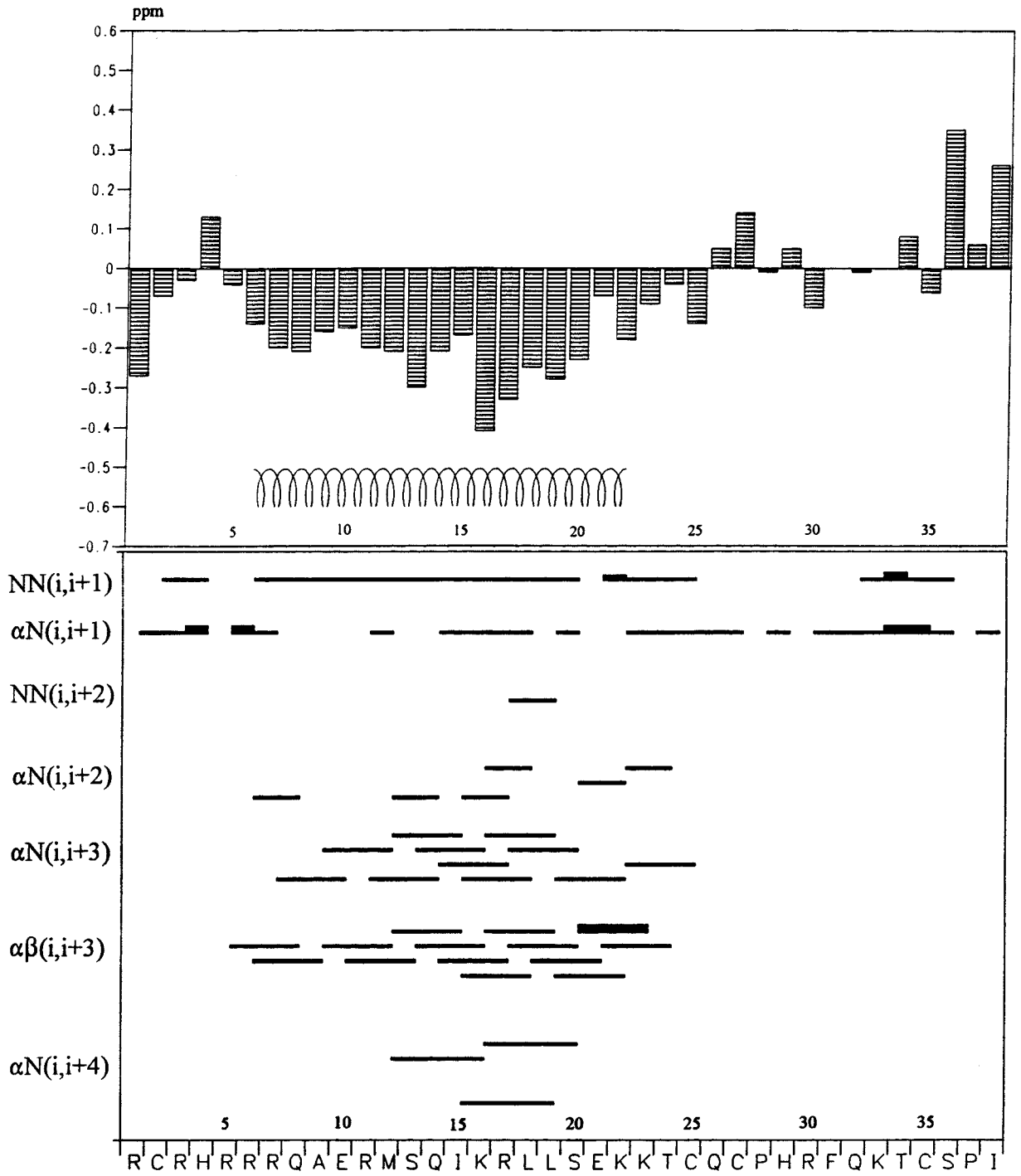

FIGURE 4: Chemical shift differences (ppm) of the α-protons between the experimental values in 50% TFE and those for residues in a random coil for $CD4_{CYTO}$ (upper panel), and summary of the observed NOEs for $CD4_{CYTO}$ (lower panel).

β-strands. Wishart et al. (*36*) have shown that this provides a quick and reliable criterion for locating secondary structure. Hence, helices are present when four adjacent residues show upfield shifts greater than 0.1 ppm, while downfield shifts of three adjacent residues greater than 0.1 ppm are indicative of a *β*-strand. Figure 4A (top panel) shows the situation found for $CD4_{CYTO}$. According to the above criterion, the peptide forms an α-helix between Arg-6 and Cys-25.

Qualitatively similar conclusions regarding the position of the helix emerge from inspection of the medium-range NOE data (Figure 4B). The absence of any long-range NOE's implies that $CD4_{CYTO}$ assumes a linear structure with an α-helix centered toward the N-terminus, a short flexible N-terminus, and a longer nonstructured C-terminus.

Final Structures from Simulated Annealing and Refinement Calculations. A total of 212 distance restraints based on the quantitative NOE data (60 intraresidue, 100 sequential, and 52 medium-range NOEs) were used to generate 100 conformations. The best 20 of these, in which there was no NOE distance violation greater than 0.01 nm and for which the NOE energy term was lower than 5 kJ/mol and the total energy was below 257 kJ/mol, were chosen for the final alignment analysis. The regions of stable structure were assessed using the consecutive segment approach described

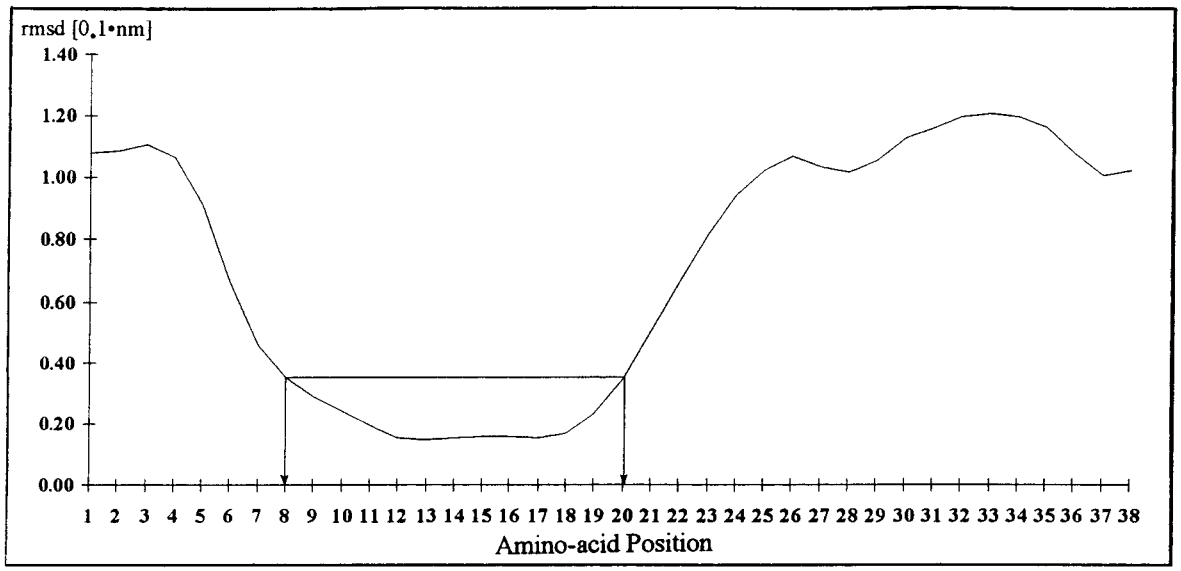

FIGURE 5: Mean RMS differences (Å) for backbone atoms in each residue of $CD4_{CYTO}$, calculated by the consecutive segment method, plotted against the residue number. The arrows correspond to the end residues used for the fitting in Figure 6.

by us previously (*34*) in which the RMS differences for short segments two, three, four, and five residues in length were systematically compared pairwise for all selected final structures. The average RMS differences for all the backbone atoms were assigned to all residues in the segment chosen, and subsequently the mean value was calculated for each residue after all segment lengths and all structures had been computed. These mean RMS differences were then plotted against the residue number and afford an objective visual assessment of how well the backbone atom positions in each amino acid in all the final refined structures are defined. The result of this analysis for $CD4_{CYTO}$ is shown in Figure 6. In keeping with the qualitative analyses, one stable structural element is found in the N-terminal section of the peptide. The sharp increase in the RMS function at the N-terminus (residues 1−5) and over the greater part of the C-terminus (residues 24−38) is unambiguous evidence of nonstructured regions in the peptide under these experimental conditions. For a meaningful fitting of the final structures, only residues with similiar low RMS functions should be included. Here we have arbitrarily chosen to fit regions between residues with RMS functions below 0.04 nm in Figure 5, i.e., between residues 8 and 20. All structures were then fitted pairwise with all other structures using initially that structure with the lowest mean RMS deviation as template to give the stereoview superpositions shown in Figure 6. These clearly demonstrate that the structured region possesses an α-helix centered in the region chosen for fitting between Gln-8 and Ser-20. This continues toward either end, at least to Arg-7 and Lys-22, but soon after becomes much less well defined. Inspection of this region (Arg-7 to Lys-22 in peptide $CD4_{CYTO}$, residues 402−417 in the intact CD4 molecule), visualized in Figure 6B−D by looking along the helical axis, indicates the presence of an amphipathic helix with the hydrophobic residues (Ala-9, Met-12, Ile-15, Leu-18, and Leu-19) segregated evenly to one side of the entire helix in opposition to the various types of hydrophilic residues.

As is the case with many studies of small peptides, the type of calculation procedure we have used must overestimate the stability of the helical conformation. Inspection of the NOE data (Figure 4) shows that the relative intensities of the sequential $d_{\alpha N}$ NOEs compared to the d_{NN} NOEs and the medium-range $d_{\alpha N}(i,i+3)$ NOEs compared to $d_{\alpha\beta}(i,i+3)$ are stronger than expected for an ideal stable helix (*37*). This must be attributed to the occurrence of a dynamic equilibrium between helical and nonhelical structures. The r^{-6} dependence of the NOE strongly favors compact structures in an ensemble of structures, but this does not imply that other structures are not present. Thus, the convergence of our structural calculation to a low RMS difference does not necessarily mean that the calculated structures accurately represent the ensemble of conformations in solution. In addition to the relative intensities of the experimental NOE cross-peaks, two further independent lines of evidence suggest that the fractional population of helical conformations in solution is indeed less than unity. The CD curves shown in Figure 3 indicate that the fractional helicity of the peptide continues to increase at TFE percentages greater than the value of 50% used in the NMR experiments and, more convincingly, the Hα chemical shift differences in the helical region (Figure 4) are less than the mean value of −0.39 ppm found for such protons in a stable helical configuration (*38*). Although the changes in the CD curves may also arise from stabilization of helical conformations outside the helical region found from the NOE data, this is not the case with the chemical shift data as this provides direct access to the positions of interest, namely, residues 8−20. Alternative methods of assessing this phenomenon involving the use of the ratio of the sequential NOEs or vicinal coupling constants between the amide and α-protons are not possible here due to incomplete data sets or unavailable data, respectively.

Hence, using the mean Hα chemical shift difference for the region Gln-8 to Ser-20 of −0.24 ppm, the fractional population of helical conformations in this region is 62% on average with individual residue occupancies being highest in the region of residues 16−19.

Thus, in summary, both the qualitative and quantitative Hα chemical shift difference data and NOE data provide convincing evidence that on average the cytoplasmic domain

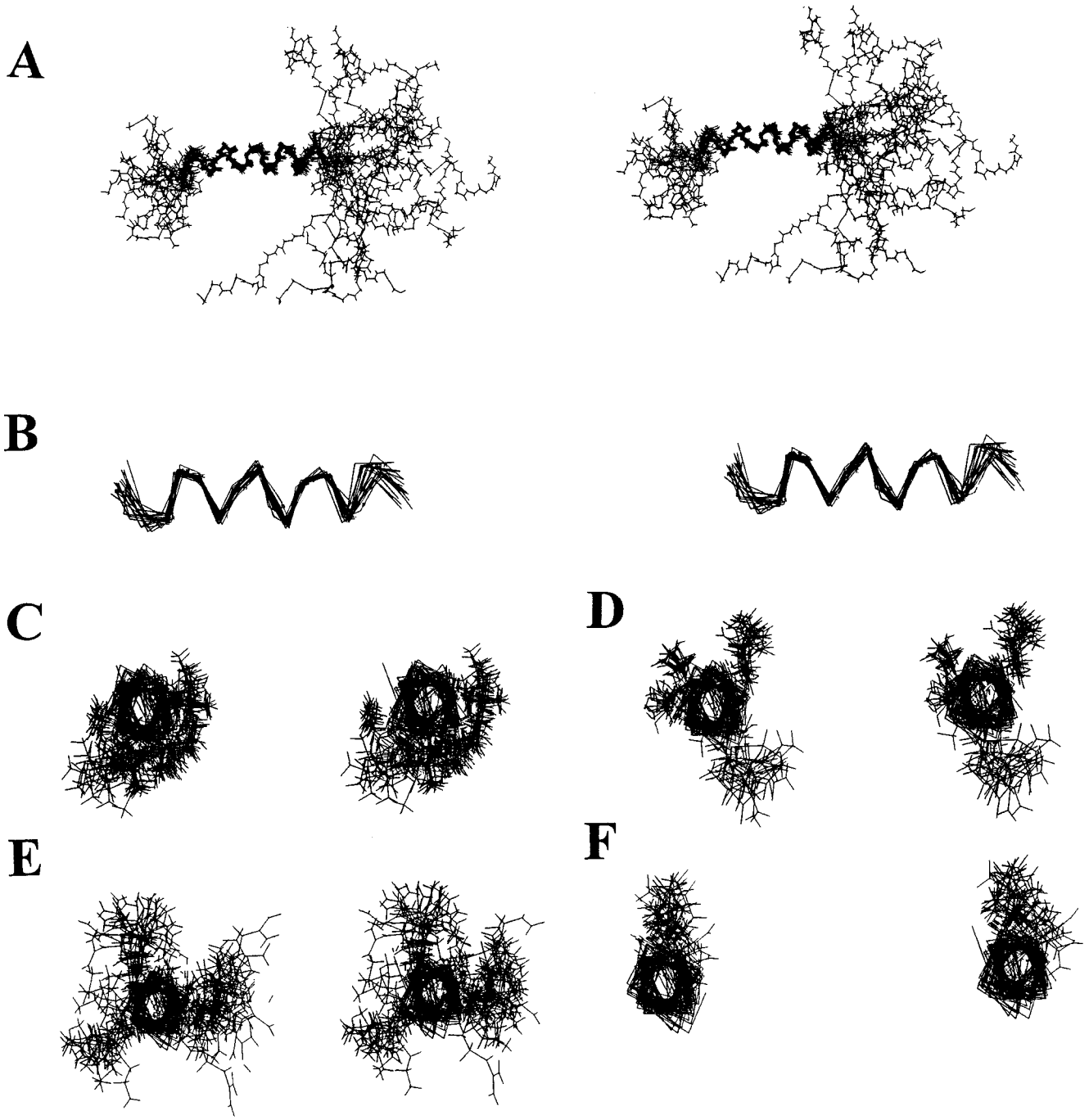

FIGURE 6: Stereoview superposition of the 20 best final restrained structures of $CD4_{CYTO}$ in 50% TFE after alignment of the backbone atoms of Gln-8 to Ser-20. (A) Full structure with backbone atoms; (B) secondary structure from Arg-7 to Lys-22 showing helix fraying; (C) as in (A) but only region Arg-7 to Lys-22 viewed through the helix with residue 7 in front and displaying hydrophobic side chains; (D−F) as in (C) but displaying neutral, positive, and negatively charged hydrophilic side chains, respectively.

of CD4 consists of a dynamic equilibrium of conformations in which the predominant structural feature is an α-helix approximately 4 turns in length between residues 8 and 20 that leads, on the C-terminal side, into a rather long nonstructured region approximately 14−18 residues in length. This begins before the cysteine residue at position 25 that is known to be important for binding of $p56^{lck}$ to CD4.

DISCUSSION

Solution Structure of $CD4_{CYTO}$. Even though extensive structural investigations have been published for the $CD4_{ECTO}$ domain (*1*), the present work is the first time that the solution structure of another entire functional domain of CD4 has been solved. $CD4_{CYTO}$ has features typical of a membrane-associated protein, in that it comprises an amphipathic helix with terminal flexible structures under limiting solution conditions. The α-helix is specifically located in the N-terminal half of $CD4_{CYTO}$ and centered between Gln-8 and Ser-20 that corresponds to residues 403 and 415 of the intact CD4 molecule (*39*). It is connected at the N-terminal side by a short mobile linker to the anchor region $CD4_{TM}$ and at the C-terminal side to an unusually long unstructured region. The latter is approximately 14−18 residues in length and remains unstructured under all solution conditions tested. Although $CD4_{CYTO}$ consists primarily of hydrophilic residues,

it is surprising that no other stable structure was found apart from the short 4 turn helix. No folding of the $CD4_{CYTO}$ was observed as judged from the absence of long-range NOEs; hence, we assume that $CD4_{CYTO}$ adopts an extended structure with a N-terminal helical core structure. The absence of tertiary folds under our conditions, again, underlines the previously reported observation (*40*) that the four cysteine residues do not participate in disulfide bond formation which could otherwise stabilize potential loop formation in $CD4_{CYTO}$.

Our finding that $CD4_{CYTO}$ only adopts a stable α-helical core structure in TFE implies that the cytoplasmic tail of CD4 has the propensity to adopt a stable structure on close contact with the membrane while it appears to be largely unstructured when it extends into the cytoplasmic space. The crucial question now arises whether the cytoplasmic tail of CD4 has the potential to interact with the membrane. Our data for the interaction of in vitro phosphorylated $CD4_{CYTO}$ with canine microsomal membranes indicate that this is indeed the case and that approximately 60−70% of the peptide remains membrane-associated. This result justifies our structural approach and implies that the helical core identified may reflect the actual structure of the cytoplasmic domain of CD4 in vivo. However, our current studies cannot give details about the position of $CD4_{CYTO}$ at the membrane. In addition, our experimental conditions are for several reasons only a crude approximation of those pertaining in the cellular environment. For instance, our analysis cannot take into account the cytoplasmic conditions (pH, salt concentrations, oxidative potential) or the presence of the $CD4_{ECTO}$ and $CD4_{TM}$ domains or the CD4-binding proteins, of which three (Nef, Vpu, and $p56^{lck}$) are known to be directly involved in interactions with $CD4_{CYTO}$. The importance of PKC phosphorylation for the interaction of $CD4_{CYTO}$ with the ER membrane also requires further clarification. However, both the qualitative and quantitative NMR data provide convincing evidence for the presence of predominantly α-helical secondary structure upon increasing the content of TFE. Furthermore, our data provide reliable experimental evidence that only a fraction of the complete $CD4_{CYTO}$ tail has the ability of adopting stabilized helical structure in an environment that exists at or near the membrane surface and that this structure is located in the membrane-proximal region.

Correlation of the Structure with Other Published Data. Recently, a study of an *N*-acetyl 17 amino acid N-terminal fragment of $CD4_{CYTO}$ (residues 403−419) has shown that a loose helical region exists between Gln-403 and Arg-412 even when this peptide was studied in aqueous solution in the absence of organic solvents (*41*). This contrasts with the findings for our 38 amino acid peptide where there was very little evidence of secondary structure in water alone. Thus, the helical region appears to be more stable in the smaller N-terminal fragment of $CD4_{CYTO}$ studied by Willbold and Rösch (*41*) than in the full-length cytoplasmic domain evaluated here. It is, therefore, conceivable that the N- and C-terminal regions, which are inherently nonstructured, destabilize the α-helical core structure. These findings, taken in the context of our results for full-length $CD4_{CYTO}$, indicate that addition of TFE causes a stabilization of the helical region in the molecule that already has a tendency for such a structure when this helical region of $CD4_{CYTO}$ was studied

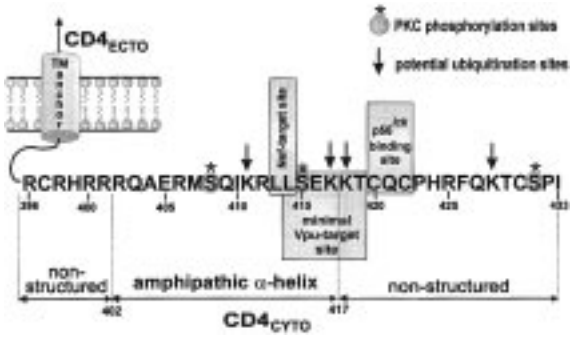

FIGURE 7: Schematic showing the correlation of the structure and main interaction regions of the cytoplasmic domain of CD4.

in water alone (*41*). However, in the context of full-length $CD4_{CYTO}$, the helical core structure requires stabilizing factors which could be provided either by the membrane itself or by other CD4 interacting factors such as Vpu, Nef, or $p56^{lck}$.

Implications of the $CD4_{CYTO}$ Structure for Interaction with Other Proteins. $CD4_{CYTO}$ is known to interact with two HIV accessory proteins, Nef and Vpu, and the $p56^{lck}$ kinase (Figure 7). Of particular interest is the interaction between the cytoplasmic domains of the two type I integral membrane proteins, CD4 and Vpu, which share striking structural similarities. As with $CD4_{CYTO}$, the structure of the 50 amino acid Vpu_{CYTO} domain, the binding partner of CD4 $_{CYTO}$ in the process of Vpu-mediated CD4 degradation (*2*), has also been analyzed under similar solution conditions, i.e., 50% TFE, by CD and NMR spectroscopy (*42*, *43*). Under these conditions, Vpu_{CYTO} adopts a well-defined helix−interconnection−helix−turn conformation, a structure which was in most details confirmed by others using a 42 amino acid fragment of Vpu_{CYTO} in 0.5 N salt solution without organic solvents (*44*). Thus, as both cytoplasmic domains of Vpu and CD4 are already in the vicinity of the cytosolic leaflet of the ER membrane through attachment by their membrane anchors and both show α-helical structures when analyzed in isolation, there is good reason to believe that both partners will have adopted stabilized secondary structure before mutual binding at the ER membrane.

Mutational analyses (*5*, *24*) suggest that putative α-helical structures in both binding partners, $CD4_{CYTO}$ and Vpu_{CYTO}, are required for their interaction during Vpu-induced CD4 degradation. It seems, therefore, intriguing that the initial step in this process requires the binding of membrane-proximal amphipathic helices predicted (*3*, *5*, *24*) and demonstrated by solution NMR experiments for the cytoplasmic domains of both, CD4 and Vpu. Since CD4−Vpu binding is required but not sufficient to induce degradation of CD4 (*2*), it is conceivable that the helical interaction is the first event in the multistep process leading to Vpu-mediated CD4 proteolysis. This interaction occurs independently of the presence of a second amphipathic helix identified in Vpu_{CYTO} (*24*, *42*, *43*) and also independently of the phosphorylation of two CK-2 phosphoacceptor sites in positions Ser^{52} and Ser^{56} in Vpu_{CYTO}, although both criteria are necessary to complete the degradation of CD4 after initial binding between Vpu and CD4 (*24*, *27*, *45*, *46*).

We demonstrated recently that the Vpu-induced proteolysis of CD4 requires the function of cytosolic proteasomes and the ubiquitin-conjugating pathway (*47*). Many of the

substrates of the 26S proteasome carry multimers of Ub, a 76 amino acid peptide, attached to the ϵ-amino group of Lys residues. The $CD4_{CYTO}$ tail can be potentially exposed to enzymes of the cellular Ub system. Substitution of the four Lys residues of $CD4_{CYTO}$ by Arg prevented CD4 degradation, suggesting that polyubiquitination of one or more Lys residues in the $CD4_{CYTO}$ domain is required for the Vpu-induced CD4 degradation (*47*). It is noteworthy that three of the potential ubiquitination sites (Lys in positions 411, 417, and 418 of CD4) are located within the α-helical core region, while Lys-429 of CD4 resides within the mobile C-terminal end of CD4 (Figure 7). Further studies are necessary to investigate the consequence of polyubiquitination at these Lys residues for the structure of $CD4_{CYTO}$ and its interaction with other membrane associated factors.

Similarly to the Vpu−CD4 interaction, it was also implicated from site-directed mutagenesis that the helical structure in $CD4_{CYTO}$ (*17*) in addition to a di-leucine motif located within this structure (*16*) is required in the Nef-induced endocytosis of CD4. In contrast to Vpu, the HIV accessory protein Nef is not a type I integral membrane protein but is attached to the inner leaflet of the cell membrane by N-terminal myristoylation (*11*). Heteronuclear NMR spectroscopy on complexes of Nef with a 13-residue fragment of $CD4_{CYTO}$ incorporating the di-leucine motif and most of the helical region (*48*) provided clear evidence for the structural constraints required in the Nef−CD4 interaction. However, these studies did not examine the consequence of the membrane environment on the CD4−Nef interaction and were performed solely with short CD4 peptides whose structures were not analyzed.

$CD4_{CYTO}$ is known to interact with a third binding partner, the tyrosine kinase $p56^{lck}$ which like Nef is associated with the cell membrane through N-terminal myristoylation (*49*). The structural constraint for this interaction is not as well characterized as that required for the binding of CD4 with the HIV proteins Nef and Vpu. Recently, mutational analyses demonstrated that the closely neighboring cysteine residues in positions 20 and 23 of the $p56^{lck}$ N-terminus and in positions 25 and 27 of $CD4_{CYTO}$ are important for the CD4−$p56^{lck}$ interaction (*9*, *40*, *50*). Since both di-cysteine motifs are not involved in the formation of disulfide bridges, it has been speculated that the CD4−$p56^{lck}$ complex is stabilized by chelate complex formation with Zn^{2+} ions (*50*). From our experiments, we would conclude that both cysteine residues are located outside the helix identified in $CD4_{CYTO}$ and within a highly flexible region that would allow formation of the predicted chelate complex. Similar to interaction with Nef and Vpu, phosphorylation of $CD4_{CYTO}$ is not required for $p56^{lck}$−CD4 binding (*21*), but a stable helical framework (*4*) in $CD4_{CYTO}$ appears to be one necessary criterion.

Consequently, the central role of CD4 in the immune response and the importance of interactions of its cytoplasmic domain with other cellular and viral factors suggest future structural analyses of $CD4_{CYTO}$ in a membrane system, for instance by heteronuclear solid-state NMR techniques, and in association with the binding partners Vpu, Nef, and $p56^{lck}$. Such studies should shed more light on the key molecular mechanisms of T cell activation and HIV-mediated receptor interference.

ACKNOWLEDGMENT

We thank J. W. Yewdell and J. R. Bennink for support, J. A. Frelinger for helpful comments on the manuscript, and H. P. W. Fischer for technical assistance.

SUPPORTING INFORMATION AVAILABLE

Table of ^1H chemical shifts and assignments for $CD4_{CYTO}$ in 50 vol % TFE at 300 K and pH 1.91 (2 pages). Ordering information is given on any current masthead page.

REFERENCES

1. König, R., Fleury, S., and Germain, R. N. (1996) in *The CD4 molecule. Roles in T lymphocytes and in HIV disease* (Littman, D. R., Ed.) pp 19−47, Springer, Berlin.
2. Bour, S., Schubert, U., and Strebel, K. (1995) *J. Virol. 69*, 1510−1520.
3. Shin, J., Dunbrack, R. L., Lee, S., and Strominger, J. L. (1991) *J. Mol. Biol. 266*, 10658−10665.
4. Gratton, S., Yao, X.-J., Venkatesan, S., Cohen, E. A., and Sékaly, R.-P. (1996) *J. Immunol. 157*, 3305−3311.
5. Yao, X.-J., Friborg, J., Chrecroune, F., Gratton, S., Boisvert, F., Sékaly, R. P., and Cohen, E. A. (1995) *Virology 209*, 615−623.
6. Bour, S., Geleziunas, R., and Wainberg, M. A. (1995) *Microbiol. Rev. 59*, 63−93.
7. Veilette, A., Bookman, M. A., Horack, E. M., and Bolen, J. B. (1988) *Cell 55*, 301−308.
8. Glaichenhaus, N., Shastri, N., Littman, D. R., and Turner, J. M. (1991) *Cell 64*, 511−520.
9. Shin, J., Doyle, C., Yang, Z., Kappes, D., and Strominger, J. L. (1990) *EMBO J. 9*, 425−434.
10. Pelchen-Matthews, A., Parsons, I. J., and Marsh, M. (1993) *J. Exp. Med. 178*, 1209−1222.
11. Trono, D. (1995) *Cell 82*, 189−192.
12. Buonocore, L., and Rose, J. K. (1990) *Nature 345*, 625−628.
13. Crise, B., Buonocore, L., and Rose, J. K. (1990) *J. Virol. 64*, 5585−5593.
14. Willey, R. L., Maldarelli, F., Martin, M. A., and Strebel K. (1992) *J. Virol. 66*, 226−234.
15. Willey, R. L., Maldarelli, F., Martin, M. A., and Strebel, K. (1992) *J. Virol. 66*, 7193−7200.
16. Aiken, C., Konner, J., Landau, N. R., Lenburg, M. E., and Trono, D. (1994) *Cell 76*, 853−864.
17. Anderson, S. J., Lenburg, M., Landau, N. R., and Garcia, J. V. (1994) *J. Virol. 68*, 3092−3101.
18. Garcia, J. V., and Miller, D. (1991) *Nature 350*, 508−511.
19. Mangasarian, A., Foti, M., Aiken, C., Chin, D., Carpentier, J.-L., and Trono, D. (1997) *Immunity 6*, 67−77.
20. Chen, M. Y., Maldarelli, F., Karczewski, M. K., Willey, R. L., and Strebel, K. (1993) *J. Virol. 67*, 3877−3884.
21. Lenburg, M. E., and Landau, N. R. (1993) *J. Virol. 67*, 7238−7245.
22. Willey, R. L., Buckler-White, A., and Strebel, K. (1994) *J. Virol. 68*, 1207−1212.
23. Raja, N. U., Vincent, M. J., and Jabbar, M. A. (1994) *Virology 204*, 357−366.
24. Tiganos, E., Yao, X.-J., Friborg, J., Daniel, N., and Cohen, E. A. (1997) *J. Virol. 71*, 4452−4460.
25. Shaw, A. S., Amrein, K. E., Hammond, C., Stern, D. F., Sefton, B. M., and Rose, J. K. (1989) *Cell 59*, 627−636.
26. Maddon, P. J., Littman, D. R., Godfrey, M., Maddon, D. E., Chess, L., and Axel, R. (1985) *Cell 42*, 93−104.
27. Schubert, U., and Strebel, K. (1994) *J. Virol. 68*, 2260−2271.
28. Wray, V., Kakoschke, C., Nokihara, K., and Naruse, S. (1993) *Biochemistry 32*, 5832−5841.
29. Niedig, K. P., and Kalbitzer, H. R. (1990) *J. Magn. Reson. 88*, 155−160.
30. Brünger, A. T. (1992) *X-PLOR, Version 3.1, A System for X-ray Crystallography and NMR*, Yale University Press, New Haven and London.

31. Nilges, M., Clore, G. M., and Gronenborn, A. M. (1988) *FEBS Lett. 239*, 129−136.
32. Weber, P. L., Morrison, R., and Hare, D. (1988) *J. Mol. Biol. 204*, 483−487.
33. Schomburg, D., and Reichelt, J. (1988)*J. Mol. Graphics 6*, 161−165.
34. Blankenfeldt, W., Nokihara, K., Naruse, S., Lessel, U., Schomburg, D., and Wray, V. (1996) *Biochemistry 35*, 5955−5962.
35. Gesell, J., Zasloff, M., and Opella, S. (1997) *J. Biomol. NMR 9*, 127−135.
36. Wishart, D. S., Sykes, B. D., and Richards, F. M. (1992) *Biochemistry 31*, 1647−1651.
37. Wagner, G., Neuhaus, D., Wörgötter, E., Vasak, M., Kägi, J. H. R., and Wüthrich, K. (1986) *J. Mol. Biol. 187*, 131−135.
38. Wishart, D. S., Sykes, B. D., and Richards, F. M. (1991) *J. Mol. Biol. 222*, 311−333.
39. Maddon, P. J, Molineaux, S. M., Maddon, D. E., Zimmermann, K. A., Godfrey, M., Alt, F. W., Chess, L., and Axel, R. (1987) *Proc. Natl. Acad. Sci. U.S.A. 84*, 9155−9159.
40. Shaw, A. S., Chalupny, J., Whitney, J. A., Hammond, C., Amrein, K. E., Kavathas, P., Sefton, B. M., and Rose, J. K. (1990) *Mol. Cell. Biol. 10*, 1853−1862.
41. Willbold, D., and Rösch, P. (1996) *J. Biomed. Sci. 3*, 435−441.
42. Wray, V., Federau, T., Henklein, P., Klabunde, S., Kunert, O., Schomburg, D., and Schubert, U. (1995) *Int. J. Pept. Protein Res. 45*, 35−43.
43. Federau, T., Schubert, U., Flossdorf, J., Henklein, P., Schomburg, D., and Wray, V. (1996) *Int. J. Pept. Protein Res. 47*, 297−310.
44. Willbold, D., Hoffmann, S., and Rösch, P. (1997) *Eur. J. Biochem. 245*, 581−588.
45. Schubert, U., Schneider, T., Henklein, P., Hoffmann, K., Berthold, E., Hauser, H., Pauli, G., and Porstmann, T. (1992) *Eur. J. Biochem. 204*, 875−883.
46. Schubert, U., Bour, S., Ferrer-Montiel, V., Montal, M., Maldarelli, F., and Strebel, K. (1996) *J. Virol. 70*, 809−819.
47. Schubert, U., Anton, L. C., Bacik, I., Cox, J. H., Bour, S., Bennink, J. R., Orlowski, M., Strebel, K., and Yewdell, J. W. (1998) *J. Virol.* (in press).
48. Grzesiek, S., Stahl, S. J., Wingfield, P. T., and Bax, A. (1996) *Biochemistry 35*, 10256−10261.
49. Geleziunas, R., Bour, S., and Wainberg, M. A. (1994) *FASEB J. 8*, 593−600.
50. Turner, J., Brodsky, M. H., Irving, B. A., Levin, S. D., Perlmutter, R. M., and Littman, D. R. (1990) *Cell 60*, 755−765.

BI9723111